Review

Targeted Nanotheranostics for Future Personalized Medicine: Recent Progress in Cancer Therapy

Sung Duk Jo[1*], Sook Hee Ku[1*], You-Yeon Won[1,2], Sun Hwa Kim[1✉], and Ick Chan Kwon[1,3✉]

1. Center for Theragnosis, Biomedical Research Institute, Korea Institute of Science and Technology (KIST), 5 Hwarang-ro 14-gil, Seongbuk-gu, Seoul 02792, Republic of Korea.
2. School of Chemical Engineering, and Purdue University Center for Cancer Research, Purdue University, West Lafayette, IN 47907, USA.
3. KU-KIST School, Korea University, 145 Anam-ro, Seongbuk-gu, Seoul02841, Republic of Korea.

*These authors contributed equally to this work.

✉ Corresponding authors: Sun Hwa Kim, PhD, Phone: +82-2-958-6639, E-mail: sunkim@kist.re.kr. Ick Chan Kwon, PhD, Phone: +82-2-958-5912, E-mail: ikwon@kist.re.kr.

Abstract

Recently, many theranostic nanomaterials have been developed by integrating therapeutic and diagnostic agents in a single regimen. Real-time visualization of nano drug carrier biodistributions, drug release processes and therapeutic responses can provide critical information needed for dynamically optimizing treatment operations in a personalized manner in real time. This review highlights recent progresses in the development of multifunctional nanoparticles possessing both therapeutic and imaging functionalities for cancer therapy. The advantages of using nanoparticle platforms are discussed. Examples demonstrating various combinations of imaging and therapeutic modalities are highlighted.

Key words: Nanotheranostics, Personalized medicine, Cancer therapy.

1. Introduction

Theranostics is an emerging therapeutic paradigm that enables simultaneous implementation of therapy and diagnosis [1, 2]. By combining both therapeutic and diagnostic functions in one delivery formulation, theranostic agents enable disease diagnosis, therapy, and real-time monitoring of treatment progress and efficacy, all with one pharmaceutical agent. Due to the heterogeneous nature of cancer [3], one type of treatment is effective only for a subset of the patient population. The capability to monitor drug accumulation in target tissues and therapeutic responses enables an individualized feedback process whereby treatment strategies (drug doses, patient management protocols, etc.) are further adjusted to meet the changing needs of each patient [4]. Therefore, theranostics is an enabling technology for personalized medicine.

Recent advances in nanomaterials technology have prompted developments of many theranostic agents containing both therapeutic and imaging functions [5, 6]. It is generally considered that using nanoscale carriers is critical to achieving long blood circulation (by escaping both renal clearance and hepatic capture) and high accumulation in tumor tissue. Tumors typically have leaky vasculature and impaired lymphatic drainage, resulting in higher permeation and longer retention of nanoparticles. This passive targeting mechanism, known as the enhanced permeability and retention (EPR) effect, has been widely cited as a rationale for using nanocarriers in cancer therapy [7, 8]. Physicochemical characteristics of nanoparticles, such as size, shape and surface chemistry, are critical for tumor-specific accumulation. Rigid nanoparticles with sizes in the range 100 – 200 nm have prolonged blood circulation times because they are large enough to avoid renal clearance but at the same time small enough to avoid capture by the reticuloendothelial system (RES) [9].

Particle shape is also known to affect cellular uptake. However, an optimal nanoparticle shape for maximal tumor accumulation and cellular uptake has not been determined because the effect of particle shape is also coupled with particle size [9, 10]. Surface chemistry influences both systemic-level processes (such as opsonization) and cellular-level processes (such as cell uptake). Cationic surface charges enhance cellular uptake of nanoparticles due to increased electrostatic interactions with cell membranes, while at the systemic level, positive charges can cause opsonization, i.e., adsorption of serum proteins, and subsequent clearance in the RES [10]. Protein adsorption can be prevented by functionalization with poly(ethylene glycol) ("PEGylation"), which thereby renders nanoparticles "stealthy", i.e., undetectable by the immune system [11]. End-grafted PEG chains provide a steric barrier against protein adsorption [12], and the effect of PEGylation on the stability of nanoparticles depends on PEG chain length and grafting density [13, 14]. Furthermore, surface functionalization of nanoparticles with active targeting ligands (such as antibodies, peptides or aptamers) can enhance the accumulation of the nanoparticles in tumors and also the subsequent internalization of the nanoparticles by cancer cells [8].

For theranostic applications, various combinations of therapeutic and imaging modalities are possible. Noninvasive imaging methods (including optical, magnetic resonance (MR), computed topography (CT), positron emission tomography (PET) and ultrasonic (US) imaging techniques) can be used to monitor the biodistribution, drug release kinetics and therapeutic efficacy of theranostic nanoparticles [15, 16]. Nanotheranostic approaches can be realized using various therapeutic strategies, such as chemotherapy, gene therapy, photodynamic therapy (PDT), and photothermal therapy (PTT) [17]. In this article, we review recent demonstrations of synergistic effects of combining these various types of therapeutic and imaging capabilities into single nanoparticle embodiments (Table 1).

Table 1. Theranostic technologies for cancer treatment.

Imaging method	Carrier material	Imaging agent	Therapeutic agent	Function	Ref.
Optical imaging	Glycol chitosan	Cy5.5	Paclitaxel	Real time tracking of NP location	[24]
	Mesoporous silica NP	FITC-coumarin pair	Doxorubicin	Drug release monitoring	[26]
	PEG-PLA[a]	Dicyanomethylene-4H-pyran	Camptothecin	Drug release monitoring	[27]
	(PPEGMA-b-PESPMA)[b]	Cy7, ^{111}In	Cyclophosphamide, etopside	Real time imaging of apoptosis	[31, 32]
	Hyaluronic acid	Cy5.5-BHQ pair	Doxorubicin	Real time imaging of apoptosis	[33]
	Glycol chitosan	Ce6	Ce6	Real time tracking of NP location & PDT	[36]
	Hyaluronic acid	Ce6-BHQ pair	Ce6	Drug release monitoring & PDT	[37]
	UCNP[c] (β-NaYF$_4$:Yb^{3+},Er^{3+})	UCNP (β-NaYF$_4$:Yb^{3+},Er^{3+})	Cisplatin prodrug	Imaging of NP location	[41]
	UCNP (NaYF$_4$:Er)	UCNP (NaYF$_4$:Er)	TPGS[d]	Dual imaging (optical, CT) & reducing multidrug resistance	[42]
	UCNP (NaYF4:Yb/Er)	UCNP (NaYF4:Yb/Er)	Ce6, doxorubicin	Imaging of particle location & chemotherapy/PDT	[44]
MR imaging	PEG liposome	Gd	Doxorubicin	Real time monitoring of drug delivery	[50]
	FA-PEG-SPION[e] Nanocluster	SPION	SPION	Detection & hyperthermia treatment of tumor	[54]
	Poly(TMSMA-r-PEGMA-r-NAS)[f]-coated SPION	SPION	Doxorubicin	Tumor detection & chemotherapy	[55]
	PEI[g]-coated silica NP	SPION/FITC	siRNA	MR imaging & gene therapy	[57]
CT imaging	Aptamer-conjugated GNP[h]	GNP	Doxorubicin	CT imaging of cancer & chemotherapy	[60]
	Silica-modified GNR[i]	GNR	GNR	Dual imaging (X-ray/CT) & PTT/radiosensitization	[65]
PET imaging	H40-P(LG-Hyd-DOX)-b-PEG	^{64}Cu	Doxorubicin	Quantitative biodistribution analysis & chemotherapy	[67]
	Cyclodextrin	^{64}Cu	siRNA	Quantitative determination of biodistribution & efficacy of siRNA NPs	[68]
US imaging	Glycol chitosan	Perfluoropentane	Docetaxel	Triggered drug release & chemotherapy	[73]
	PEG-PAsp[k]	CaCO$_3$	Doxorubicin	Tumor imaging & triggered drug release	[75]
	PLGA[l]	Perfluorooctyl bromide	Camptothecin	Chemotherapy & ablation therapy	[82]
	Mesoporous silica NP	Perfluorohexane	CPT11[m]	Tumor imaging & chemotherapy/ablation therapy	[83]

[a]poly(ethylene glycol)-poly(lactic acid), [b]poly(PEG-methacrylate)-*b*-poly(triethoxysilyl propylmethacrylate), [c]upconverting nanoparticle, [d]tocopheryl polyethylene glycol 1000 succinate, [e]superparamagnetic iron oxide nanoparticle, [f]poly 3-(trimethoxysilyl)propyl methacrylate-r-PEG methyl ether methacrylate-r- N-Acryloxysuccinimide, [g]polyethyleneimine, [h]gold nanoparticle, [i]gold nanorod, [j]Boltorn® H40-poly(L-glutamate-hydrazone-doxorubicin)-block-poly(ethylene glycol), [k]poly(ethylene glycol)-block-poly(L-aspartic acid), [l]poly(lactic-co-glycolic acid), [m]irinotecan hydrochloride trihydrate.

2. Nanotheranostic optical imaging

Fluorescence and bioluminescence optical imaging techniques have attracted much interest because of their high sensitivity and cost-effectiveness. Near-infrared (NIR) (λ = 650 – 950 nm) fluorescence imaging has been widely used for in vivo optical imaging because NIR offers high tissue penetration depths (on the order of millimeters) compared to UV and visible light [18]. NIR fluorescence dyes can be incorporated into nanoparticles derived from polymers and lipids via covalent conjugation or physical encapsulation. Co-delivering NIR dyes with anticancer drugs in single nanoparticle delivery systems enables non-invasive real-time measurements of biodistribution, drug pharmacokinetics and therapeutic responses against the disease [17, 19]. If NIR photosensitizers are used, they can play an additional role as a mediator for PDT in addition to optical imaging.

2.1. Optical imaging approaches for monitoring biodistribution

Conventional anticancer drugs, such as doxorubicin (DOX) and paclitaxel (PTX), have toxic effects on normal cells. Cancer targeted delivery can mitigate this problem; nanomedicine offers hope in this regard. Incorporation of NIR fluorescent probes in nano drug carriers enables real-time in vivo tracking of the nanoparticles [20]. Our laboratories have extensively investigated tumor-homing characteristics of glycol chitosan nanoparticles (GCNPs) by NIR imaging; for these studies, a fluorescent dye, Cy5.5, was covalently conjugated to the glycol chitosan backbone [21-23]. PTX-containing Cy5.5-labeled GCNPs (PTX-Cy5.5-GCNPs) exhibited high stability and, at the same time, high deformability (Figure 1A) [24]. When PTX-Cy5.5-GCNPs were intravenously administered in SCC7 xenograft-bearing mice, strong NIR fluorescent signals were detected in tumor tissues, confirming the tumor-specific accumulation of PTX-Cy5.5-GCNPs (Figure 1B). The tumor-homing characteristics of PTX-Cy5.5-GCNPs subsequently resulted in significant suppression of tumor growth (1,000 mm^3 in treated mice vs. 8,400 mm^3 in control mice), with significantly reduced levels of PTX toxicity in normal cells (Figure 1C and 1D). Micelles have also been demonstrated to be effective delivery systems for drugs and imaging agents. Chung et al. developed micellar carriers based on peptide amphiphiles that can specifically target glioblastoma [25]. Because brain tumors are typically characterized by high levels of fibrin deposition, a fibrin-targeting peptide, cysteine-arginine-glutamic acid-lysine-alanine (CREKA), was conjugated to DSPE-PEG. A fluorescent dye, Cy7, was incorporated into the DSPE-PEG micelles for visualization. Fluorescent imaging following intravenous injection in a xenograft glioma mouse model confirmed that Cy7-CREKA-micelles accumulate in brain tumor tissue at a much higher level than non-targeting control. These studies support that nanoparticle formulations can improve tumor selectivity and efficacy, while reducing off-target effects of chemo drugs.

2.2. Optical imaging approaches for visualizing of drug release

The principle of fluorescence resonance energy transfer (FRET) can be used to visualize the drug release processes. A carrier and a drug can be labeled with a pair of fluorophores (a FRET donor and a FRET acceptor), and the energy transfer between donor and acceptor can be considered as an indicator for drug release. Lee et al. developed the FRET-based monitoring system for redox-responsive DOX release from mesoporous silica nanoparticles (MSNPs) [26]. The pores of MSNPs were are loaded with therapeutic cargo (DOX) and blocked with a molecular stopper, fluorescein isothiocyanate(FITC, FRET acceptor)-labeled β-cyclodextrin (β-CD) linked to surface-bound coumarin (FRET donor) through a disulfide bond (Figure 2A). In the absence of reducing agents, DOX remained entrapped within MSNPs, and the FRET between coumarin (λ_{ex} = 405 nm, λ_{em} = 450 nm) and FITC (λ_{ex} = 488 nm, λ_{em} = 520 nm) caused a fluorescence emission at 520 nm (under 405 nm excitation). In the glutathione(GSH)-rich, reductive cytoplasmic environment, the cleavage of the disulfide bonds resulted in the removal of the FITC-β-CD molecular stopper and the liberation of DOX by diffusion. Once nearby FITC-β-CD molecules are detached, coumarin recovers its original fluorescence character (with an emission at 450 nm under 405 nm excitation). An in vitro study confirmed that no FRET signal was observed in high GSH-containing cells, whereas high FRET intensities were observed in low GSH-containing cells (Figure 2B); there results confirmed the possibility that the FRET mechanism can be used to monitor intracellular drug release processes. Fluorescent prodrugs can also be used for similar purposes. A donor-π-acceptor structured chromophore was developed by combining a NIR fluorophore, dicyanomethylene-4H-pyran (DCM), and an anticancer drug, camptothecin (CPT), through a disulfide linker [27]. The chromophore exhibited a broad absorption at 455 nm and a weak FRET emission at 655 nm. When DCM

was detached by the cleavage of the disulfide bond, a strong NIR fluorescence was observed. In the intracellular environment the DCM-CPT prodrug produced the DCM fluorophore and the CPT drug, and this process could be monitored by NIR fluorescence imaging. In an in vivo study in mice, a strong NIR fluorescence was measured in tumor xenografts (stronger relative to other major organs such as liver, kidney, lung, and stomach) after 9 minutes following i.v. administration of PEG-PLA-encapsulated DCM-CPT nanoparticles, suggesting a rapid accumulation and internalization of the nanoparticles in tumor cells. The detailed release kinetics could be determined in real time by NIR imaging. The CPT drugs thus delivered effectively suppressed the tumor growth in mice while no body weight loss was observed.
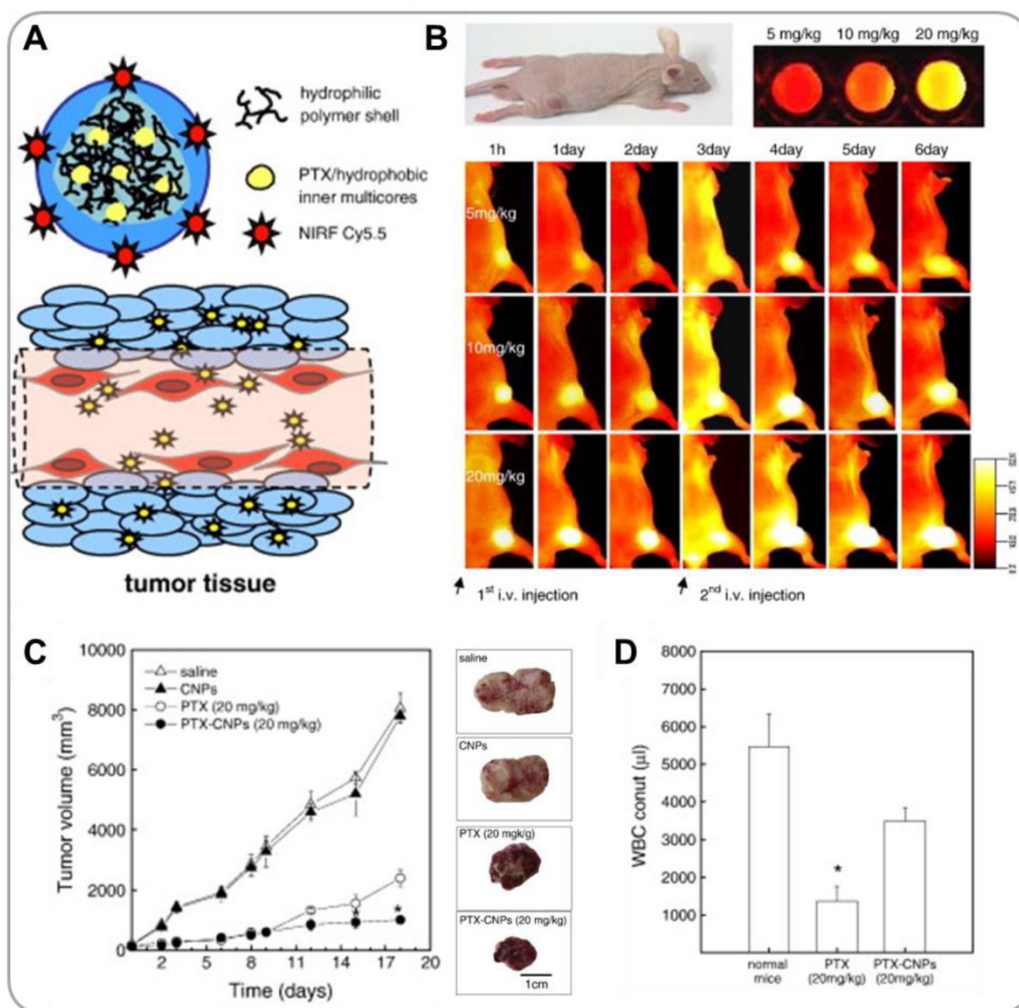

Figure 1. Glycol chitosan-based nanoparticles (GCNPs) for combining near infrared (NIR) fluorescence imaging and chemotherapy. (A) Schematic illustration of GCNPs labeled with Cy5.5 (for NIR optical imaging) containing physically loaded paclitaxel (PTX) (for chemotherapy) (PTX-Cy5.5-GCNP). (B) NIR images of tumor-bearing mice taken after i.v. injection of PTX-Cy5.5-GCNPs at different concentrations. (C) Tumor growth curves, and representative images of excised tumor tissues after repeated injections of saline, glycol chitosan nanoparticles, free PTX, and PTX-Cy5.5-GCNPs. (D) Acute toxicities of free PTX and PTX-Cy5.5-GCNPs determined by WBC counts. Reproduced with permission from reference [24].
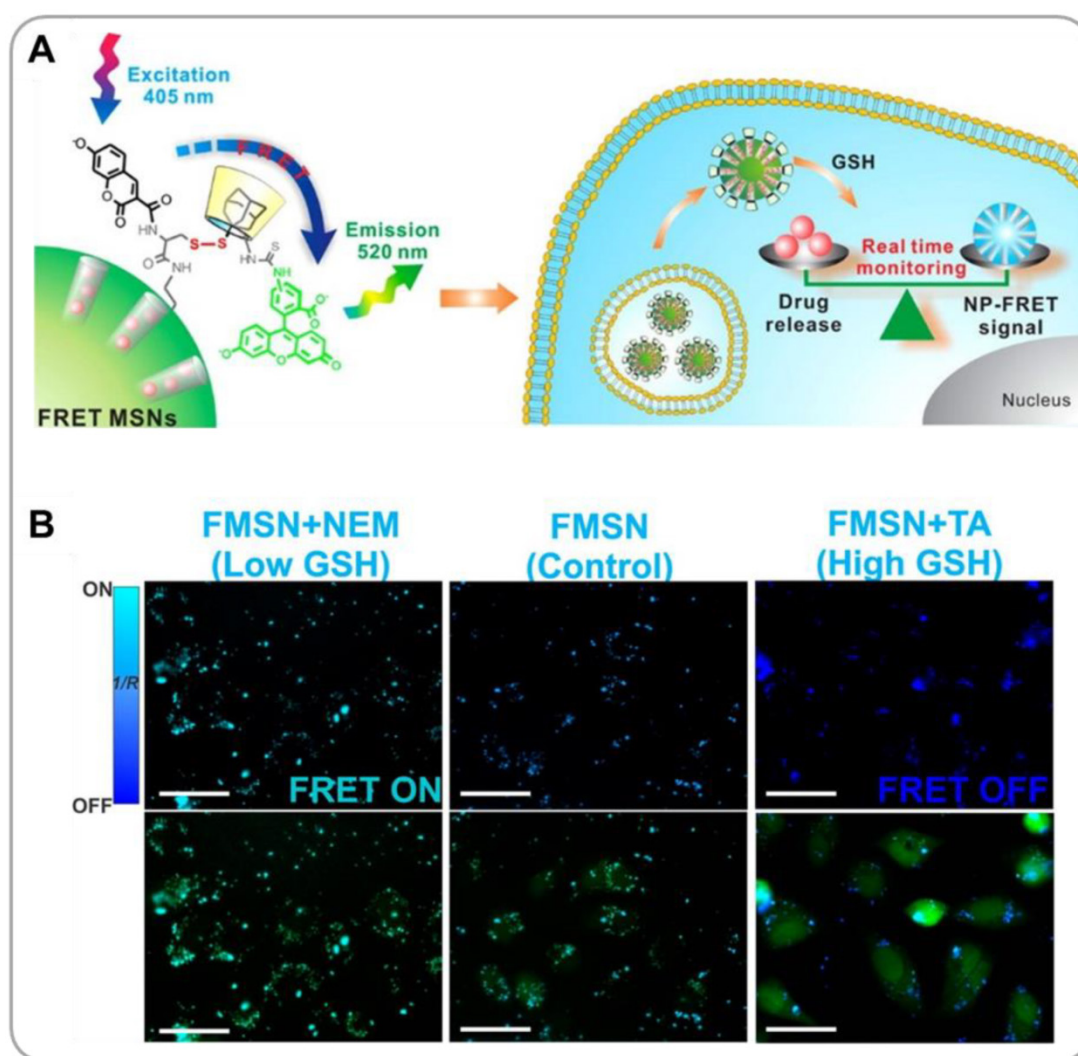
Figure 2. Mesoporous silica nanoparticles (MSNPs) for FRET-based drug release monitoring. (A) Schematic description of redox-responsive drug release and FRET detection mechanisms. (B) Representative fluorescence images of MSNP-treated cancer cells with different glutathione concentrations, taken under FRET (λ_{ex} = 405 nm) and FITC (λ_{ex} = 488 nm) channels. Reproduced with permission from reference [26].

2.3. Optical imaging approaches for measuring therapeutic efficacy

A tumor's response to chemotherapy can be monitored by optical imaging methods. Common mechanisms used for this type of measurement include the detection of changes in the composition of the plasma cell membrane [28, 29] and the detection of overexpression of certain enzymes during the cell death period [30]. Phosphatidylserine (PS) is an important lipid component of the inner leaflet of the plasma membranes of viable cells. In dying cells, PS relocates to the outer leaflet of the plasma membrane, and this process can be detected by Annexin V binding to externalized PS. Li et al. developed Annexin V-functionalized core-crosslinked polymeric micelles (A5-CCPMs) loaded with two types of imaging probes, Cy7 for NIR fluorescence imaging and ^{111}In for SPECT/CT imaging [31, 32].

Lymphoma-bearing mice were treated with cytotoxic anticancer drugs, cyclophosphamide and etoposide, and subsequently A5-CCPMs were intravenously administered to monitor the efficacy of these medications. Relative to control (tumor mice not treated with drugs), the chemo-treated group exhibited strong SPECT/NIR fluorescence signals in tumor, which confirms the apoptotic effect of the drugs in lymphoma xenografts. Active caspases are also useful markers of apoptosis [30]. Caspase-detecting nanoparticles have been prepared by loading hyaluronic acid nanoparticles (HANPs) with NIR dyes (Cy5.5) and fluorescent quencher molecules (Black Hole Quencher or BHQ); Cy5.5 was linked to BHQ by a caspase-cleavable peptide (DEVD) spacer [33]. Under the influence of caspase 3, the DEVD segment became cleaved, and a fluorescent signal was produced, which signified apoptosis. In the in vivo mouse study, DOX-treated xenografts

showed significantly higher NIR fluorescence signals (by a factor of 4.0 ± 1.3 at 30 minutes) than untreated control, confirming the occurrence of apoptosis. Taken together, NIR fluorophores are promising components for use in the development of new theranostic nanoparticle agents.

For convenient assessment of drug efficacy, a similar or identical nanoplaform that used for delivery of therapeutic agents can be loaded with imaging agents. Choi et al. reported PEG-conjugated hyaluronic acid nanoparticles (P-HA-NPs) that can be used for combining optical imaging with chemotherapy [34]. An anticancer drug, irinotecan (IRT), was loaded into the hydrophobic core of P-HA-NPs (IRT-P-HA-NPs); these nanoparticles were shown to have the capability to selectively target colon cancers and significantly suppress tumor growth in a mouse model. An NIR fluorescent dye, Cy 5.5, was chemically conjugated to produce Cy 5.5-P-HA-NPs that could be used to monitor the response of the tumor to the drug. Tumor xenografts in mice could be clearly visualized following intravenous injection of Cy 5.5-P-HA-NPs. At 40 days post-IRT-P-HA-NP treatment, the fluorescent signal from the treated group was significantly lower than controls. Using fluorescent imaging to monitor drug responses can help clinicians make informed treatment decisions/adjustments.

2.4. Simultaneous optical imaging and photodynamic therapy

Photosensitizers having absorption maxima in the far-red region can also be used as imaging agents in addition to their utility as photosensitizing agents for photodynamic therapy (PDT). Photosensitizers emit fluorescence under optical irradiation (allowing in vivo detection) and also generate reactive singlet oxygen (causing damage to cancer cells) [35]. PDT photosensitizers can be physically encapsulated or covalently conjugated to polymer nanoparticles (Figure 3A). In an in vivo study [36], it has been shown that, when physically encapsulated within GCNPs, hydrophobic photosensitizers, chlorin e6 (Ce6), were initially burst released during blood circulation, which resulted in a short blood circulation time and a poor tumor accumulation. In contrast, when covalently attached to GCNPs, Ce6 was delivered into tumor very effectively. The fluorescence property of Ce6 was used to visualize the drug delivery process in real time (Figure 3B). Further, 671-nm laser irradiation significantly suppressed tumor growth in vivo (Figures 3C and 3D) because of the production of reactive oxygen species (ROS) by Ce6. The fluorescence property of a photosensitizer can also be used to monitor the release

process under the optical microscope. Park et al. developed BHQ-functionalized HANPs for encapsulation and delivery of Ce6 [37]. Inside the HANPs the fluorescence of Ce6 was quenched by BHQ. Upon release from the nanoparticles (caused by intracellular hyaluronidases), Ce6 produced strong NIR fluorescence signals. Ce6-containing HANPs were observed to effectively accumulate in tumor tissue, be effectively internalized by cancer cells, release Ce6 in the cytoplasmic compartments and generate ROS under NIR illumination. Ce6/HANPs enabled NIR imaging of the PDT process.

2.5. Upconverting nanoparticles for optical imaging

Recently, lanthanide-based upconverting nanoparticles (UCNPs) have emerged as a new class of theranostic agents [38, 39]. UCNPs exhibit unique optical properties; they absorb low-energy NIR light and emit high-energy UV/visible photons. This upconversion luminescence mechanism has unique advantages, including resistance to photobleaching and low autofluorescence, which makes UCNPs very promising candidates for medical imaging applications [40]. Drug-loaded composite UCNP/polymer nanoparticles have been shown to be able to deliver drugs to cancer cells, and using UCNPs also allows to trace the transport pathways of the nanoparticles. Lin et al. reported that UCNPs (β-NaYF4:Yb^{3+}, Er^{3+}) assembled with cisplatin-conjugated polymer prodrugs (UCNP@P-Pt) can efficiently deliver cisplatin to cancer cells and allow the optical imaging of the delivery process in vivo (Figure 4A) [41]. After the nanoparticles were endocytosed by cells, cisplatin molecules conjugated to polymers via disulfides were released because of the reductive environment of the cytoplasm. The green emission of UCNPs under NIR excitation allowed monitoring of nanoparticle translocation (Figure 4B). The UCNP@P-Pt enabled an efficient cellular uptake of cisplatin, resulting in a more efficient killing of cancer cells than pristine cisplatin or cisplatin-conjugated polymer prodrugs alone (Figure 4C). Systemically administered UCNP@P-Pt induced necrotic cell death in cervical cancer xenografts, whereas saline-treated control exhibited negligible necrosis (Figure 4D). The UCNPs/polymer formulation has also been shown to overcome the drug resistance possessed by some tumors [42]. The surfaces of NaYbF4:Er UCNPs were functionalized with a P-glycoprotein(Pgp)-inhibiting moiety, tocopheryl polyethylene glycol 1000 succinate (TPGS). DOX was loaded onto UCNP/polymer nanocomposite particles. TPGS facilitated the accumulation of DOX in cell's cytoplasm by reducing

the Pgp expression. The green emission of UCNPs under NIR laser irradiation was used for optical imaging, and the X-ray mass attenuation coefficient of Yb simultaneously allowed CT imaging; both these methods were used to confirm the tumor accumulation of the nanoparticles. Co-delivery of TPGS and DOX resulted in effective killing of multi-drug-resistant cancer cells in vivo.

UCNPs can also be combined with photosensitizers for PDT. Liu et al. showed that Ce6-loaded UCNPs generated singlet oxygen under 980-nm NIR light, which reduced cancer cell viability and suppressed tumor growth in vivo [43]. Pristine UCNPs exhibited strong emission at two wavelengths, 550 and 660 nm, under 980-nm laser excitation. In the presence of co-encapsulated Ce6, the

red emission at 660 nm was quenched by Ce6. Therefore, the luminescence signal at 550 nm could be used for locating UCNPs, and the signal at 660 nm could be used to measure the release kinetics of Ce6 from nanoparticle carriers. Similarly, DOX/Ce6-containing UCNPs have been developed for combined chemo-PDT. Under 980-nm laser irradiation, the significant loss of cancer cell viability was observed from the DOX/Ce6/UCNPs-treated cancer cells [44]. Overall, UCNPs have attracted great interest in recent years as a theranostic agent because of their high photostability, low autofluorescence and low cytotoxicity. Also, UCNPs can be doped with lanthanide ions (such as Gd^{3+} or Sm^{3+}) for use as MRI/SPECT contrast agents [45, 46].
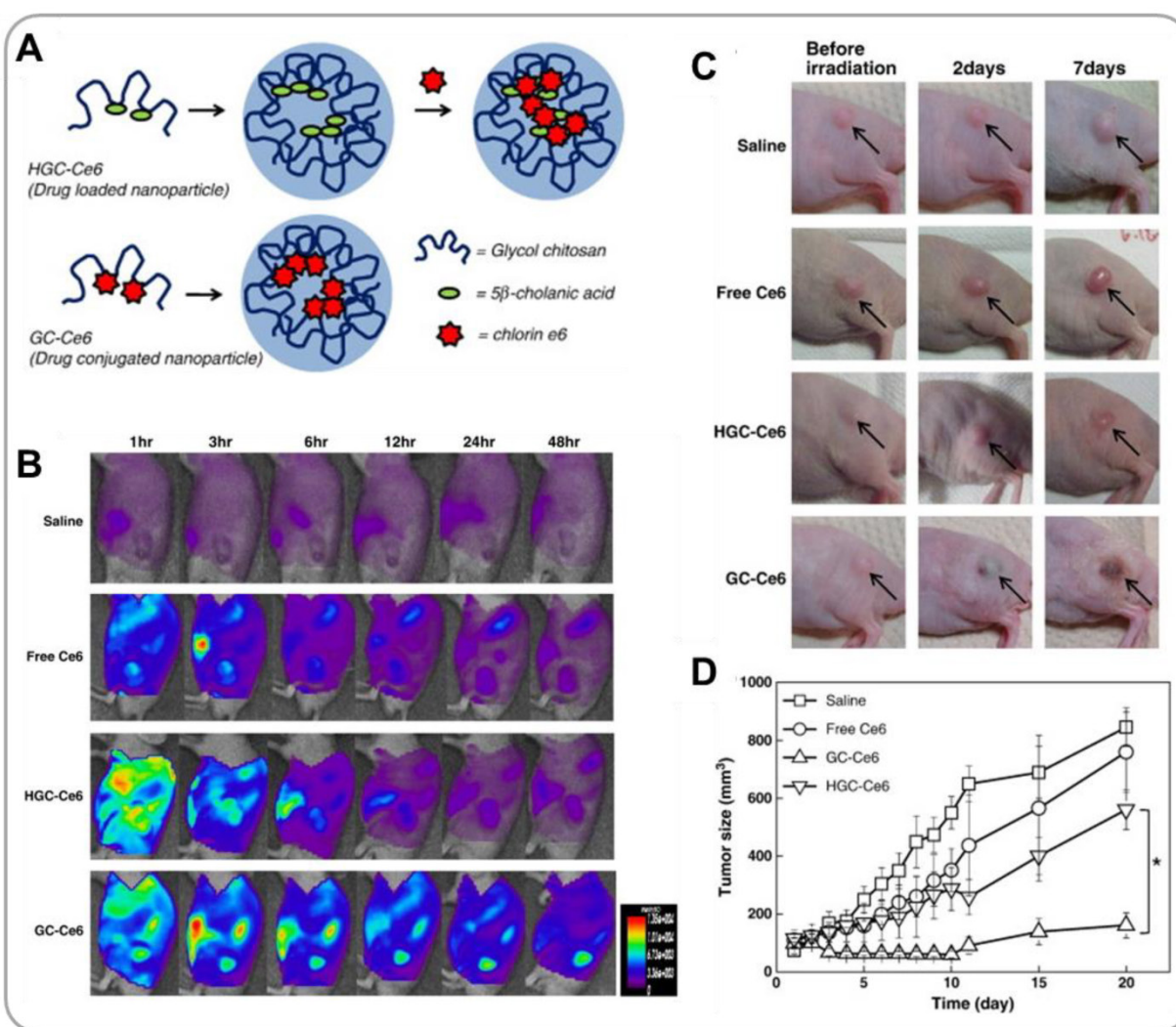

Figure 3. GCNPs for photodynamic therapy (PDT). (A) Schematic illustration of GCNPs containing physically encapsulated or chemically conjugated Ce6 photosensitizers. (B) Time series NIR images of tumor-bearing mice after i.v. injection of GCNPs. (C) Representative images of tumors, and tumor growth curves after treatments with saline, free Ce6, GCNPs containing physically entrapped Ce6, and Ce6-conjugated GCNPs. Reproduced with permission from reference [36].
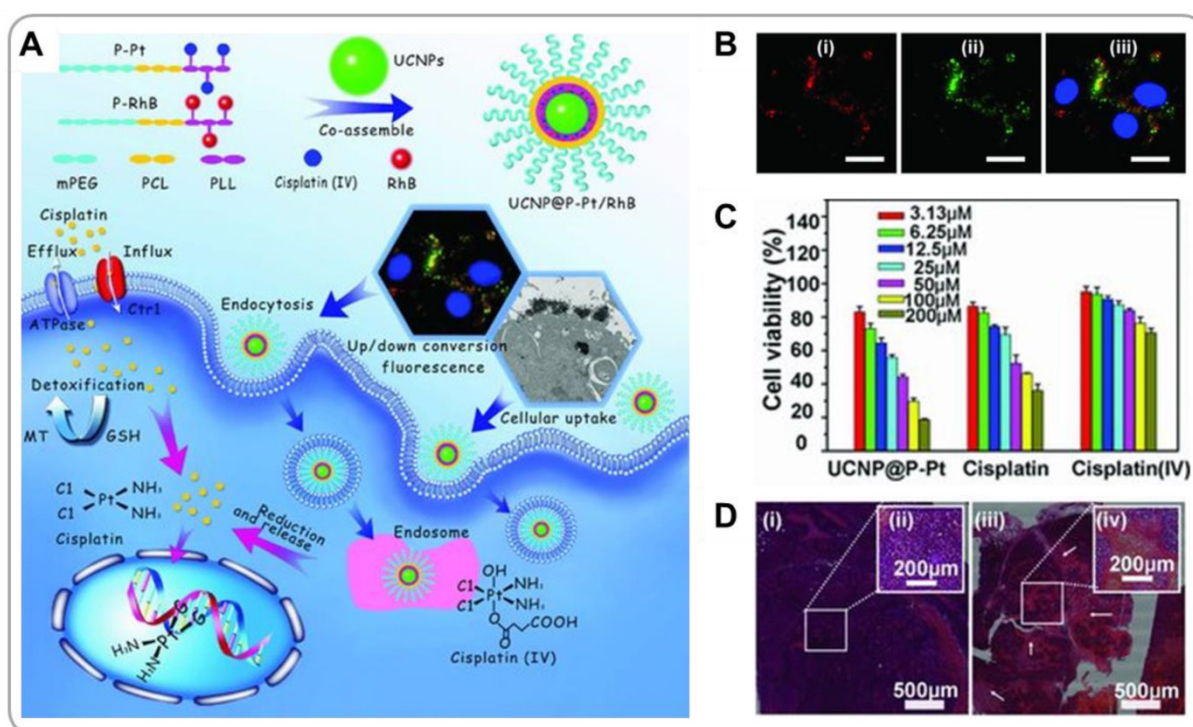
Figure 4. Upconverting nanoparticle(UCNP)/polymer composite nanoparticles for combining NIR imaging and chemotherapy. (A) Preparation of UCNPs containing cisplatin prodrugs (UCNP@P-Pt), and their intracellular mechanism of action. (B) Images of cell internalized UCNPs@P-Pt. (C) Cell viabilities measured after treatments with UCNP@P-Pt, free cisplatin, and cisplatin prodrugs. (D) Histological images of saline- or UCNP@P-Pt-treated tumors. Reproduced with permission from reference [41].

3. Nanotheranostic magnetic resonance imaging

Magnetic resonance imaging (MRI) is a powerful non-invasive imaging modality that uses magnetic fields and radio waves to obtain cross-sectional tomographic images of tissues. Compared to other imaging techniques, MRI has advantages including high spatial resolution, deep penetration, and the use of non-ionizing radiation. This technique has drawbacks such as long imaging times, relatively low sensitivity, and high costs [47]. These drawbacks can be addressed by using contrast enhancing agents. Among many available materials, gadolinium (Gd, in chelated form) and magnetic nanoparticles (MNPs, such as iron oxide NPs) are two mostly commonly used contrast agents.

3.1. Gadolinium-based theranostic agents

Recently, many MRI cancer theranostic agents have been developed [48]. Gd is the most widely used MRI T_1 contrast agent, and there are several commercial Gd MRI agents approved for human use [49]. Gd was incorporated into PEGylated liposomes along with DOX for MRI visualization of the pharmacokinetic behavior of the drug delivery system in vivo [50]. The PEG-coated liposomes were further functionalized with the neural cell adhesion molecule (NCAM)-binding peptide (C3d) for targeting NCAM-positive Kaposi's sarcoma cells. The C3d-functionalized PEGylated liposomes loaded with Gd and DOX displayed enhanced cellular uptake and thus exerted higher cytotoxic effects in NCAM-expressing Kaposi's cells than non-C3d-functionalized analogues in vitro. The accumulation of NCAM-targeting liposomes was visualized in vivo by MRI. NCAM-targeting PEGylated liposomes carrying Gd and DOX were more efficiently internalized by cancer cells than non-targeting PEG liposomes; PEG liposomes mostly remained outside the cells, i.e., in the tumor interstitial space. The higher cell internalization correlated well with higher efficacy in tumor regression. Also, the liposomal encapsulation of DOX significantly decreased the drug's systemic toxicity compared to free DOX. The Gd labeling allowed real-time MRI monitoring of the pharmacological behavior of the drug delivery system.

Genetically modified viruses are attractive nano delivery systems for therapeutic and imaging agents because of the structural uniformity, polyvalency, and easiness of cargo encapsulation and surface modification [51]. Steinmetz and coworkers developed a supramolecular MRI contrast agent using tobacco mosaic virus (TMV) nanoparticles as a template [52]. The exterior tyrosine residues and the

interior glutamic acid residues of TMV coat proteins were conjugated with 1,4,7,10-tetraazacyclododecane-1,4,7,10-tetraacetic acid(DOTA)-Gd. The TMV-immobilized DOTA-Gd showed higher relaxivity than free DOTA-Gd in solution due to reduced tumbling rates. Interestingly, the originally rod-shaped TMV particles (300 nm × 18 nm) changed to spherical shape (170 $\pm$ 41 nm diameter) after heat treatment at 96 ºC. This rod-to-sphere transition involved in an enhancement in T_1 relaxivity per Gd. Although further study is needed on such issues as potential immunogenicity and drug loading efficiency, this study demonstrates the potential utility of viral nanocarriers in theranostic applications.

3.2 Magnetic nanoparticle-based theranostic agents

Superparamagnetic iron oxide nanoparticles (SPIONs) have attracted great interest as MRI T_2 contrast agents because of their biological inertness (relative to many T_1 MRI agents). SPIONs have also been recognized as mediators for hyperthermia treatment because SPIONs generate heat under alternating magnetic fields. This magnetic hyperthermia enables selective ablation of tumor tissue with minimal collateral damage to normal tissue [53]. Folic acid (FA)-functionalized PEGylated SPION nanoclusters have been developed for combining MRI with hyperthermia [54]. Allyl-functionalized SPIONs of 7 – 9 nm diameter were PEGylated via Thiol-End Click (TEC) chemistry using bifunctional thiol-PEG-FA; this reaction produced PEGylated SPION nanoclusters of 89 nm diameter (FA-PEG-SPION NCs) (Figure 5A). FA-PEG-SPION NCs showed much higher relaxivity compared to the commercial MRI agent, Resovist, at equivalent iron concentrations. Following i.v. administration, FA-PEG-SPON NCs efficiently accumulated in tumor tissues and produced strong MRI signal intensity (Figure 5B). Moreover, by applying an alternating magnetic field the tumor tissue could be heated by 6 ºC within 20 minutes, which resulted in significant inhibition of tumor growth with no hepatotoxicity or nephrotoxicity observed (Figure 5C).

Anticancer drugs can be loaded in SPIONs for combining MRI and chemotherapy. DOX-loaded SPIONs have been developed [55]. Antibiofouling polymer-coated SPIONs were prepared by a thermal crosslinking method (TCL-SPIONs). Positively charged DOX molecules were incorporated into the negatively charged polymer shells of TCL-SPIONs by electrostatic interactions. MRI confirmed that DOX-loaded TCL-SPIONs (DOX@TCL-SPIONs)

having a hydrodynamic diameter of 21 nm significantly accumulated in tumor xenografts following i.v. injection due to the EPR effect. When delivered by TCL-SPIONs, a larger amount of DOX was delivered to tumor than free DOX. Selective accumulation of nanoparticles enhanced therapeutic efficacy with minimal systemic toxicity.

Development of safe and efficient delivery systems is a critical challenge in gene therapy [56]. SPIONs can be used as carriers for therapeutic genetic materials; SPIONs are submicron-sized, and their surfaces can readily be functionalized with various chemical groups. Yang et al. demonstrated SPION-based shRNA delivery systems for combining MRI and gene therapy [57]. Silica-coated Fe_3O_4 nanoparticles ($Fe_3O_4@SiO_2$) were further coated with FA-functionalized polyethylenimine (PEI-FA) by electrostatic adsorption (Figure 5D). Positive PEI-coated $Fe_3O_4@SiO_2$ formed complexes with negative shRNA. These complexes provided shRNA protection against degradation by nucleases. This $Fe_3O_4@SiO_2$/PEI-FA/Notch1-shRNA system was able to target specifically deliver shRNA to folate receptor overexpressing MDA-MB-321 cells, and sequence specifically silence the target gene (Notch1) in vitro; Notch1 is known to facilitate survival and proliferation of cancer cells. The down regulation of Notch1 significantly inhibited proliferation and induced apoptosis of MDA-MB-231 cells (Figure 5F). T_2-weighted MR images showed significant contrast enhancement in $Fe_3O_4@SiO_2$/PEI-FA/Notch1-shRNA-treated cells relative to untreated control (Figure 5E). This study demonstrated the potential utility of iron oxide nanoparticles for combined MRI and cancer gene therapy.

4. Nanotheranostic X-ray computed tomography

Computed tomography (CT) is one of the most widely used diagnostic imaging modalities that utilizes computerized X-ray images to produce cross-sectional tomographic images. The CT images are far more informative than conventional X-ray projections, and can also be used to construct three-dimensional displays by stacking cross-sectioned images [58]. Due to the lack of natural contrast between different tissues, it is often necessary to use contrast agents to highlight structures for functional imaging.

Gold nanoparticles (GNPs) have recently been studied extensively as potential CT contrast agents [59]. Gold (Au) is chemically stable and has a high X-ray mass attenuation coefficient. GNPs are easy to synthesize. Also, GNPs can easily be surface functionalized with various functional groups. Kim et

al. has developed GNPs functionalized with tumor targeting moieties and chemotherapeutic agents for combining CT and chemotherapy for treatment of prostate cancer [60]. The surfaces of GNPs were coated with the prostate-specific membrane antigen (PSMA) aptamer via gold-sulfur-driven assembly processes. Aptamers are small ligands that bind to specific target molecules with strong affinity and high specificity [61]. The PSMA aptamer used had an additional $(CGA)_7$ DNA duplex extension into which DOX was inserted by intercalation (Figure 6A). The GC-rich duplex region enhanced the loading of DOX relative to the original PSMA aptamer without this fragment by more than 10 folds. PSMA

aptamer-functionalized GNPs were able to bind specifically to LNCaP prostate cancer cells which overexpress PSMA. CT images of LNCaP cells (a CT value of 130 ± 17 in Hounsfield Units) treated with PSMA aptamer-conjugated GNPs showed far greater X-ray contrast than PSMA-non-expressing PC3 cells (a CT value of 28 ± 3 in Hounsfield Units) treated with the same nanoparticles (Figure 6B). Furthermore, PSMA aptamer-conjugated GNPs were able to effectively deliver DOX to LNCaP cells and induce significant cytotoxicity in those cells in vitro (Figure 6C). Multifunctional GNPs are useful platforms for combining CT and targeted chemotherapy.
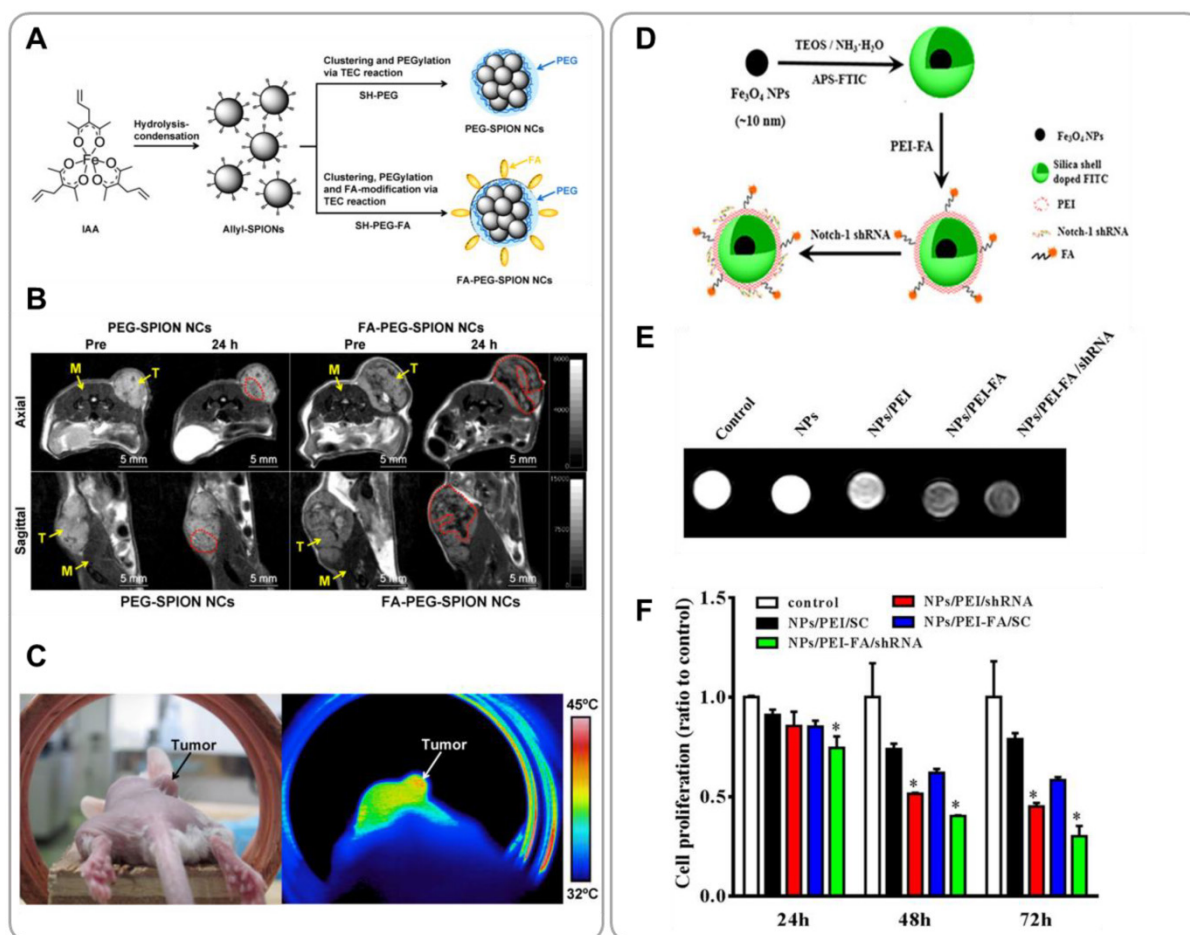

Figure 5. SPION-based nanoparticles for combining MRI and cancer therapy. (A) Schematic illustration of SPION nanoparticle clusters with (FA-PEG-SPION NCs) or without (PEG-SPION NCs) folic acid targeting moieties for combined cancer MRI and hyperthermia. (B) T_2 MR images of mice treated with i.v. injection of PEG-SPION NCs and FA-PEG-SPION NCs. (C) A thermal image of a tumor-bearing mouse after i.v. injection of FA-PEG-SPION NCs taken under an alternating magnetic field. Reproduced with permission from reference [54]. (D) Synthesis of FA-functionalized PEI-coated $Fe_3O_4@SiO_2$ nanoparticles for combining MRI and RNAi therapy ($Fe_3O_4@SiO_2/PEI-FA/Notch1-shRNA$). (E) MR images of MDA-MB-431 cells treated with $Fe_3O_4@SiO_2/PEI-FA/Notch1-shRNA$ nanoparticles or controls for 6 h. (F) Proliferation rates of MDA-MB-231 cells treated with $Fe_3O_4@SiO_2/PEI-FA/Notch1-shRNA$ nanoparticles or controls. Reproduced with permission from reference [57].
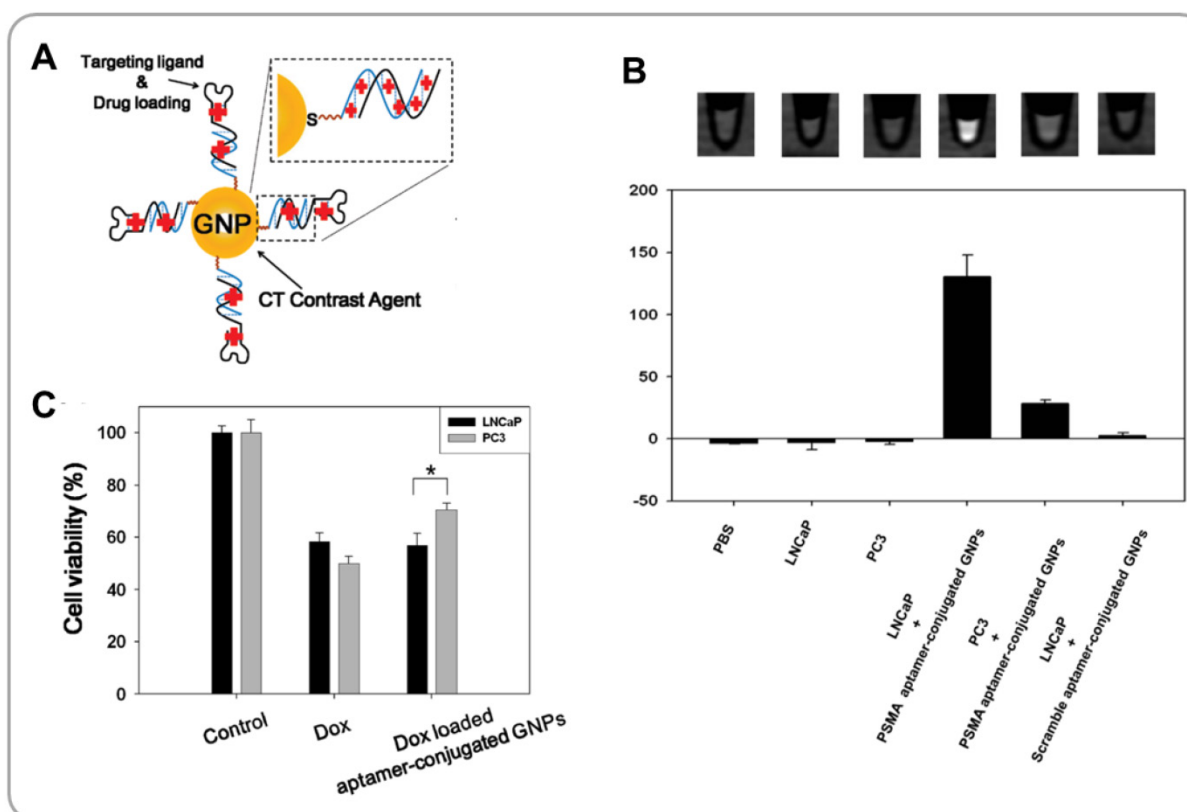
Figure 6. Functionalized gold nanoparticles (GNPs) for combining CT and chemotherapy. (A) Schematic illustration of aptamer-functionalized anticancer drug-loaded gold nanoparticles (GNPs). (B) CT images and HU values of various cells treated with aptamer-conjugated GNPs for 6 h. (C) Viabilities of cancer cells treated with doxorubicin-loaded aptamer-conjugated GNPs and controls. Reproduced with permission from reference [60].

GNPs can also be used as hyperthermia agents for cancer treatment [62]. Under optical illumination with appropriate wavelengths, GNPs produce heat that can be used to destroy the tumor. Furthermore, GNPs have the potential for use as radiosensitizers for enhancing the efficacy of radiotherapy [63, 64]. Silica-coated gold nanorods (GNRs) functionalized with targeting ligands were developed for CT-guided radiotherapy plus photothermal therapy (PTT) [65]. Because silica is chemically stable and biologically inert, cetyltrimethylammonium bromide (CTAB) surfactants on as-synthesized GNRs were replaced with silica to reduce cytotoxicity and improve biocompatibility. A tumor-targeting ligand, folic acid (FA), was conjugated to GNR-SiO$_2$. GNR-SiO$_2$-FA showed selectivity to FA receptor-overexpressing cells and induced hyperthermic death of cancer cells under NIR irradiation. GNR-SiO$_2$-FA significantly increased the cell killing effects of X-rays, confirming the radio-sensitizing capability of GNRs. In vivo CT images taken from mice injected with GNR-SiO$_2$-FA showed great contrast enhancement due to the strong X-ray mass attenuation coefficient of Au. GNR-SiO$_2$-FA is promising for use in combining CT, hyperthermia and radiotherapy.

5. Nanotheranostic positron emission tomography

Positron emission tomography (PET) is a non-invasive scanning technique that provides three-dimensional functional images of the body. Due to its high sensitivity, non-invasiveness and quantitative real-time imaging capability, PET has become an essential tool that helps physicians gauge treatment effects and make adjustments in treatment [66]. Xiao et al. developed multifunctional nanoparticle PET contrast agents with additional capabilities for tumor targeting and drug loading [67]. In order to provide needed in vivo stability to self-assembled polymer micelles, a unimolecular micelle was prepared from a hyperbranched amphiphilic block copolymer, Boltorn® H40-poly(L-glutamate-hydrazone-doxorubicin)-block -poly(ethylene glycol) (H40-P(LG-Hyd-DOX)-b-PEG). DOX was conjugated to the polymer via low pH-cleavable hydrazone bonds for tumor-specific release of the drug. The branched polymer was also functionalized with cRGD peptides (for targeting integrins on the tumor neovasculature) and with 1,4,7-triazacyclononane-N,N',N''-triacetic acid (NOTA) chelators for labeling with ^{64}Cu for PET

measurements (H40-DOX-cRGD). The average diameter of the resulting multifunctional unimolecular micelles was 65 nm, and the amount of DOX loaded was 16.2%. The hydrazone bonds were stable at physiological pH (pH 7.4), but at pH 5.3 greater than 90% of loaded DOX was released within 45 h. This pH sensitivity is necessary for achieving tumor-specific release and minimizing off-target effects of DOX given that tumors are acidic. cRGD-functionalized unimolecule micelles (H40-DOX-cRGD) demonstrated much higher cellular uptake in U87MG cancer cells than non-cRGD-functionalized micelles (H40-DOX); the cRGD-integrin interaction facilitated the endocytosis of the micelles, which led to significantly enhanced killing of cancer cells. In U87MG tumor-bearing mice, PET images taken from mice i.v. injected with ^{64}Cu-labeled H40-DOX-cRGD confirmed high accumulation of the nanoparticles in the tumor. Quantitative analysis suggested that H40-DOX-cRGD was taken up predominantly by the liver initially, and the tumor uptake of the cRGD-functionalized micelles was significantly higher than non-functionalized control or when mice were pre-treated with cRGD blocking agents. ^{64}Cu-labeled H40-DOX-cRGD can enable PET to be used to monitor the pharmacokinetics of DOX in treated patients.

Nanoparticles accumulate in tumor tissues in high concentrations and in normal tissues in low concentrations because of the EPR effect. Because drugs should reach the intracellular locations of the cancer cells for therapeutic actions, tumor tissue accumulation does not always correlate with cancer cell internalization and eventual therapeutic efficacy. Combined PET and bioluminescence imaging techniques were used to evaluate the interrelationship between the biodistribution and efficacy of siRNA nanoparticles in vivo [68]. PEGylated cyclodextrin polycation/siRNA nanocomplexes with or without transferrin (Tf) functionalization were developed. For PET imaging, the 5' end of anti-luciferase siRNA was functionalized with 1,4,7,10-tetraazacyclododecane-1,4,7,10-tetraacetic acid (DOTA) for chelation with [64]Cu. Tf-functionalized and non-functionalized siRNA nanoparticles were intravenously administered to mice bearing luciferase-expressing Neuro2A tumors. Quantitative analysis showed comparable biodistribution, pharmacokinetic and tumor accumulation profiles between Tf-functionalized and non-functionalized nanoparticles. However, the gene silencing efficacy of Tf-functionalized siRNA nanoparticles was significantly higher than non-functionalized siRNA nanoparticles. This result suggests that Tf enabled more efficient cellular entry of nanoparticles than in its absence. This study demonstrated that ^{64}Cu-labeled polyplexes can be used for combining PET and RNA interference therapy.

6. Nanotheranostic ultrasound imaging

Ultrasound (US) imaging is one of the most widely used medical imaging methods. US is non-invasive and low cost compared with other imaging techniques. US can penetrate into deep tissue and produce images in real time. US does not use ionizing radiation nor require radio-labeling [47]. In US imaging, it is often desirable to use contrast agents to improve image quality. Microbubbles are the most commonly used ultrasound contrast agents (UCAs) [69, 70]. However, conventional microbubble UCAs are too large to accumulate in tumor tissue [71]. Also, microbubbles have very short half-lives in blood [71]. Because of these limitations, conventional microbubble UCAs cannot be used for imaging tumors.

6.1. In situ gas-generating materials

Efforts have been made to develop UCAs for cancer imaging [72]. Submicron-size bubbles cannot be used as cancer UCAs because the echo signal intensity of nanobubbles is normally not sufficient; the echo signal intensity is inversely proportional to the sizes of the bubbles. To address this challenge, several in-situ gas generation methods have been proposed. Min et al. developed (tumor-homing) glycol chitosan nanoparticles loaded with gas-generating liquid-phase perfluoropentane (PFP) and anticancer drugs for combining US imaging and chemotherapy [73]. These echogenic chitosan nanoparticles (Echo-CNPs) were prepared by self-assembly of hydrophobic 5b-cholanic acid-modified glycol chitosans. Anticancer drugs (doxorubicin or docetalxel) were encapsulated within chitosan nanoparticles during the self-assembly process (Figure 7A). PFP-containing Echo-CNPs were prepared by an oil-in-water (O/W) emulsion method. The average diameter of drug/PFP-containing Echo-CNPs was 432 ± 32 nm; even at this relatively large size the fluffy chitosan nanoparticles were still able to accumulate effectively in tumor tissue due to the EPR effect [74]. The size of drug/PFP-containing Echo-CNPs increased to 2 μm at 37°C (Figure 7B). The tumor targeting capability of drug/PFP-containing Echo-CNPs was confirmed in mouse xenografts of murine squamous cell carcinoma (SCC7) following i.v. administration. Tumor accumulation of Echo-CNPs was increased by 4 – 7 folds when US was applied to the tumor after the particles were injected. This result suggests that acoustic cavitation enhances extravasation of nanoparticles into tumor tissue.

Echo-CNPs showed sustained production of microbubbles at body temperature; echogenicity was sustained for a longer period of time relative to conventional UCAs such as lipid-based Sonovue®. Echo-CNPs can also be used for delivery of anticancer drugs. The timing and location of drug release could be controlled by US. The effects of US were two folds; US enhanced tumor tissue permeability and also increased drug release, resulting in greater overall efficacy of Echo-CNPs (Figure 7C). Echo-CNPs are promising for use in US-assisted chemotherapy.

Min et al. developed gas-generating mineral nanoparticles for US/chemotherapy [75]. DOX-loaded calcium carbonate ($CaCO_3$) nanoparticles (DOX-$CaCO_3$-MNPs) were prepared by mineralization of organic block copolymer templates (Figure 7D and 7E). $CaCO_3$ dissolves and generates CO_2 in acidic solution [76]. An anionic block copolymer, poly(ethylene glycol)-block-poly(L-aspartic acid) (PEG-PAsP), was used as a nucleating agent for $CaCO_3$ mineralization. Cationic DOX was loaded into the $CaCO_3$ core by ionic interactions. Monodisperse spherical nanoparticles of about 200 nm diameter were obtained. DOX-$CaCO_3$-MNPs showed great colloidal stability in serum because of the PEG chains. At low pH, the CO_2 generation rate of DOX-$CaCO_3$-MNPs was significantly increased. CO_2 microbubbles were obtained through coalescence of smaller bubbles. Therefore, the US contrast due to DOX-$CaCO_3$-MNPs was significantly greater at acidic pH (Figure 7D). Tumor tissue is more acidic than normal tissue because of increased glycolysis [77, 78]. In vivo tests in mouse xenografts also confirmed that DOX-$CaCO_3$-MNPs produced CO_2 microbubbles, enabling US visualization of the tumor. The $CaCO_3$ core domain can be used as cargo space onto which drug molecules can be loaded. Drug release can be triggered by lowering pH; the solubility of $CaCO_3$ in water increases with decreasing pH [79]. It was confirmed that the DOX release rate of DOX-$CaCO_3$-MNPs was significantly greater at acidic pH than at neutral pH. The tumor suppression effects
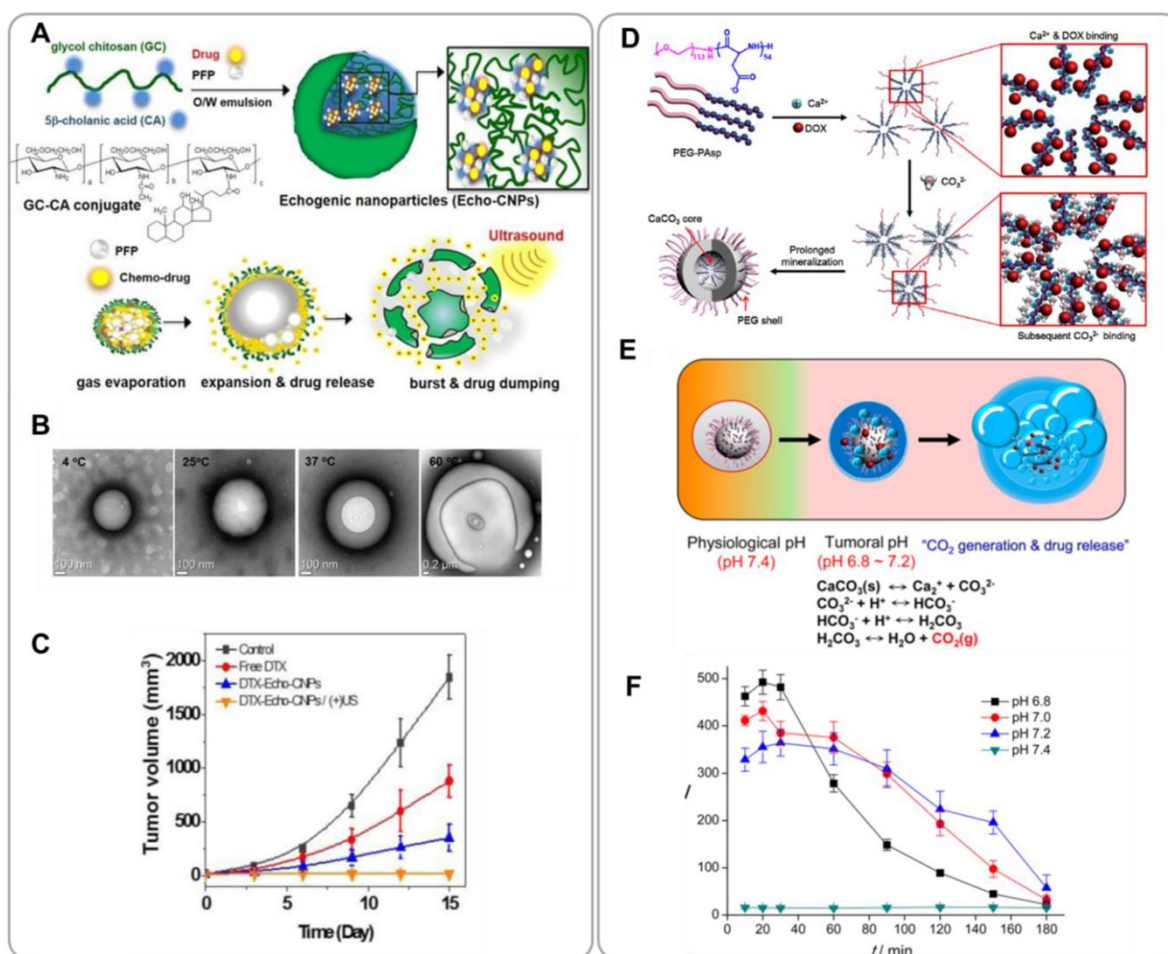

Figure 7. Theranostic nanoparticles for combining ultrasound (US) imaging and chemotherapy. (A) Schematic illustration of echogenic glycol chitosan nanoparticles (Echo-CNPs) for ultrasound-aided chemo treatment. (B) Optical microscopy images of gas bubbles formed by Echo-CNPs at various temperatures. (C) In vivo tumor suppression by docetaxel(DTX)-loaded Echo-CNPs. Reproduced with permission with reference [73]. (D) Synthesis procedures for doxorubicin-loaded $CaCO_3$ mineralized nanoparticles (DOX-$CaCO_3$-MNPs). (E) Low pH-triggered gas generation mechanism of DOX-$CaCO_3$-MNPs. (F) US contrast intensity curves of DOX-$CaCO_3$-MNPs at different pH values. Reproduced with permission from reference [75].

of DOX-CaCO$_3$-MNPs were confirmed in mouse SCC7 xenografts. DOX-CaCO$_3$-MNPs effectively accumulated in tumor tissue due to the EPR effect and enabled prolonged release of DOX within the tumor site.

6.2. High-intensity focused ultrasound-triggered controlled drug release

High-intensity focused ultrasound (HIFU) therapy is a non-invasive medical procedure that applies HIFU energy to produce heat and destroy cells locally within a target region [80]. In addition to ablation therapy, HIFU can also be used as a mechanism for locally triggering drug release [81]. For HIFU-aided chemotherapy, Shi et al. developed a HIFU-sensitive drug delivery system (DDS) [82]. By an emulsion evaporation method, a temperature-sensitive gas-generating agent perfluorooctyl bromide (PFOB) and an anticancer drug camphtothecin (CPT) were co-encapsulated into poly(lactic-co-glycolic acid) (PLGA) nanoparticles. CPT/PFOB-containing PLGA nanoparticles were then coated with an ultrathin layer of silica. These silica-coated CPT/PFOB-containing PLGA nanocapsules were further functionalized with PEG to increase colloidal stability (CPT/PFOB@SNCs). The mean hydrodynamic diameter of CPT/PFOB@SNCs was approximately 200 nm, which was appropriate for tumor accumulation. The average thickness of the silica layer was about 4 nm. The silica coating prevented an undesirable premature release of CPT. Under HIFU, however, CPT/PFOB@SNCs became ruptured, resulting in rapid release of drugs. It is believed that HIFU also increased drug diffusion, which additionally contributed to accelerated drug release. The organic/inorganic hybrid encapsulation structure allowed HIFU-controlled drug release with minimal leakage of drugs during the circulation stage. This strategy can therefore be used to reduce side effects and increase the efficacy of anticancer drugs. In vivo evaluation in VX-2 tumor-bearing rabbits showed that CPT/PFOB@SNCs effectively accumulated in tumor tissue and induced a significant level of coagulative necrosis in tumor. CPT/PFOB@SNC-treated rabbits had significantly lower numbers of proliferating cells and significantly higher numbers of apoptotic cells relative to the control group treated with non-drug-loaded nanoparticles. CPT/PFOB@SNCs demonstrated a synergistic combination of HIFU ablation therapy and chemotherapy for cancer treatment.

Similar multifunctional theranostic nanoparticles (named as MPHss-PFP for the reason described below) have also been developed using mesoporous silica nanocapsules (MSNCs) as templates [83].

MSNCs were first PEGylated, and then loaded with an anticancer drug, CPT11, and an ultrasound-sensitive gas-generating agent, perfluorohexane (PFP). Subsequently, the PEG chains were crosslinked with thiol-functionalized hyaluronic acid (HA). The resulting MPHss-PFP particles had a diameter of about 400 – 500 nm, and showed great colloidal stability, as desired for passive tumor targeting by the EPR mechanism. The HA moieties also enabled active targeting by specific ligand-receptor interactions. MPHss-PFP nanoparticles selectively targeted CD44 receptor-overexpressing HepG2 cells, which was demonstrated in vitro using CD44-null L02 cells as control. In vivo tests in mouse HepG2 xenografts also confirmed that MPHss-PFP nanoparticles effectively accumulated in tumor tissue because of the dual passive and active tumor targeting capabilities and also caused tumor ablation under HIFU excitation.

7. Conclusions

We highlight recent progresses in the development of theranostic nanoparticles for use in cancer treatment. Nanoparticles are promising for applications in cancer therapy due to their tumor-homing ability and selectivity (caused by the EPR effect). Nanoparticles can easily be surface modified to make them stealthy for the immune system and to increase their blood circulation times. Nanoparticles can easily be surface functionalized with active targeting ligands to improve their tumor-targeting efficiencies. Nanoparticles can be used as convenient platforms for constructing "All-in-One" delivery systems in which all needed functions (therapeutic, imaging, targeting, controlled release) are integrated. All-in-one nanoparticles enable to combine diagnosis, therapy and monitoring operations for treatment of cancer. Theranostic nanoparticles can be used for image-guided cancer therapy. Real-time non-invasive visualization of the tumor accumulation behavior of drugs can help define the limits of the drug's influence zone. Real-time visualization of the drug release process can help optimize the dose and schedule of the drug treatment. Real-time monitoring of therapeutic responses can provide immediate feedback regarding how well the treatment works for each patient and can thus enable to modify treatment strategies as needed. Nanotheranostics will help enable these goals toward realizing personalized cancer care. Nanotheranostics appears to be promising for personalized cancer therapy applications.

However, there are some critical issues that need to be addressed for clinical applications of theranostic nanoparticles. Since every therapeutic/imaging

modality has its own strengths and limitations, it is important to choose an optimal combination such that their combined effects are synergistic. Also, it might be challenging to optimize dose levels and frequencies simultaneously for both therapeutic and imaging agents using a single delivery regimen. In addition, when designing a nanotheranostic formulation, caution needs to be taken so that neither component (i.e., imaging and therapeutic moieties) becomes prematurely released from the delivery system; such situation would produce irrelevant, or even incorrect, information about therapeutic outcomes.

For most theranostic nanoparticle systems developed thus far, their safety in humans has not yet been studied. Nanoparticles that are structurally well-defined, reproducibly synthesizable and derived primarily from biodegradable and/or biocompatible building blocks are preferred candidates for further clinical evaluations. Deeper understanding of the mechanisms by which theranostic nanoparticles are cleared from the body and interact with the immune system is necessary. Developments of new and powerful cancer biomarkers that can be used for tumor-specific targeting and/or monitoring disease progression and responses to therapies will continue to spur the advancements of nanotheranostic technologies.

Acknowledgements

Competing Interests

The authors have declared that no competing interest exists.

References

1. Lammers T, Aime S, Hennink WE, Storm G, Kiessling F. Theranostic nanomedicine. Acc Chem Res. 2011; 44: 1029-38.
2. Rizzo LY, Theek B, Storm G, Kiessling F, Lammers T. Recent progress in nanomedicine: therapeutic, diagnostic and theranostic applications. Curr Opin Biotechnol. 2013; 24: 1159-66.
3. Burrell RA, McGranahan N, Bartek J, Swanton C. The causes and consequences of genetic heterogeneity in cancer evolution. Nature. 2013; 501: 338-45.
4. Lammers T, Rizzo LY, Storm G, Kiessling F. Personalized nanomedicine. Clin Cancer Res. 2012; 18: 4889-94.
5. Choi KY, Liu G, Lee S, Chen X. Theranostic nanoplatforms for simultaneous cancer imaging and therapy: current approaches and future perspectives. Nanoscale. 2012; 4: 330-42.
6. Xie J, Lee S, Chen X. Nanoparticle-based theranostic agents. Adv Drug Deliv Rev. 2010; 62: 1064-79.
7. Kobayashi H, Watanabe R, Choyke PL. Improving conventional enhanced permeability and retention (EPR) effects; what is the appropriate target? Theranostics. 2013; 4: 81-9.
8. Peer D, Karp JM, Hong S, FaroKHzad OC, Margalit R, Langer R. Nanocarriers as an emerging platform for cancer therapy. Nat Nanotechnol. 2007; 2: 751-60.
9. Petros RA, DeSimone JM. Strategies in the design of nanoparticles for therapeutic applications. Nat Rev Drug Discov. 2010; 9: 615-27.
10. Albanese A, Tang PS, Chan WC. The effect of nanoparticle size, shape, and surface chemistry on biological systems. Annu Rev Biomed Eng. 2012; 14: 1-16.
11. Papahadjopoulos D, Allen TM, Gabizon A, Mayhew E, Matthay K, Huang SK, et al. Sterically stabilized liposomes: improvements in pharmacokinetics and antitumor therapeutic efficacy. Proc Natl Acad Sci U S A. 1991; 88: 11460-4.
12. Hatakeyama H, Akita H, Harashima H. The polyethyleneglycol dilemma: advantage and disadvantage of PEGylation of liposomes for systemic genes and nucleic acids delivery to tumors. Biol Pharm Bull. 2013; 36: 892-9.
13. Perrault SD, Walkey C, Jennings T, Fischer HC, Chan WCW. Mediating Tumor Targeting Efficiency of Nanoparticles Through Design. Nano Lett. 2009; 9: 1909-15.
14. Perry JL, Reuter KG, Kai MP, Herlihy KP, Jones SW, Luft JC, et al. PEGylated PRINT nanoparticles: the impact of PEG density on protein binding, macrophage association, biodistribution, and pharmacokinetics. Nano Lett. 2012; 12: 5304-10.
15. Lee DE, Koo H, Sun IC, Ryu JH, Kim K, Kwon IC. Multifunctional nanoparticles for multimodal imaging and theragnosis. Chem Soc Rev. 2012; 41: 2656-72.
16. Huang Y, He S, Cao W, Cai K, Liang XJ. Biomedical nanomaterials for imaging-guided cancer therapy. Nanoscale. 2012; 4: 6135-49.
17. Ryu JH, Koo H, Sun IC, Yuk SH, Choi K, Kim K, et al. Tumor-targeting multi-functional nanoparticles for theragnosis: new paradigm for cancer therapy. Adv Drug Deliv Rev. 2012; 64: 1447-58.
18. Weissleder R. A clearer vision for in vivo imaging. Nat Biotechnol. 2001; 19: 316-7.
19. Ding H, Wu F. Image guided biodistribution and pharmacokinetic studies of theranostics. Theranostics. 2012; 2: 1040-53.
20. He X, Wang K, Cheng Z. In vivo near-infrared fluorescence imaging of cancer with nanoparticle-based probes. Wiley Interdiscip Rev Nanomed Nanobiotechnol. 2010; 2: 349-66.
21. Na JH, Koo H, Lee S, Min KH, Park K, Yoo H, et al. Real-time and non-invasive optical imaging of tumor-targeting glycol chitosan nanoparticles in various tumor models. Biomaterials. 2011; 32: 5252-61.
22. Na JH, Lee SY, Lee S, Koo H, Min KH, Jeong SY, et al. Effect of the stability and deformability of self-assembled glycol chitosan nanoparticles on tumor-targeting efficiency. J Control Release. 2012; 163: 2-9.
23. Nam HY, Kwon SM, Chung H, Lee SY, Kwon SH, Jeon H, et al. Cellular uptake mechanism and intracellular fate of hydrophobically modified glycol chitosan nanoparticles. J Control Release. 2009; 135: 259-67.
24. Kim K, Kim JH, Park H, Kim YS, Park K, Nam H, et al. Tumor-homing multifunctional nanoparticles for cancer theragnosis: Simultaneous diagnosis, drug delivery, and therapeutic monitoring. J Control Release. 2010; 146: 219-27.
25. Chung EJ, Cheng Y, Morshed R, Nord K, Han Y, Wegscheid ML, et al. Fibrin-binding, peptide amphiphile micelles for targeting glioblastoma. Biomaterials. 2014; 35: 1249-56.
26. Lai J, Shah BP, Garfunkel E, Lee KB. Versatile fluorescence resonance energy transfer-based mesoporous silica nanoparticles for real-time monitoring of drug release. ACS nano. 2013; 7: 2741-50.
27. Wu X, Sun X, Guo Z, Tang J, Shen Y, James TD, et al. In vivo and in situ tracking cancer chemotherapy by highly photostable NIR fluorescent theranostic prodrug. J Am Chem Soc. 2014; 136: 3579-88.
28. Schellenberger EA, Bogdanov A, Petrovsky A, Ntziachristos V, Weissleder R, Josephson L. Optical imaging of apoptosis as a biomarker of tumor response to chemotherapy. Neoplasia. 2003; 5: 187-92.
29. Brindle K. New approaches for imaging tumour responses to treatment. Nat Rev Cancer. 2008; 8: 94-107.
30. Riedl SJ, Shi Y. Molecular mechanisms of caspase regulation during apoptosis. Nat Rev Mol Cell Biol. 2004; 5: 897-907.
31. Zhang R, Lu W, Wen X, Huang M, Zhou M, Liang D, et al. Annexin A5-conjugated polymeric micelles for dual SPECT and optical detection of apoptosis. J Nucl Med. 2011; 52: 958-64.
32. Zhang R, Huang M, Zhou M, Wen X, Huang Q, Li C. Annexin A5-functionalized nanoparticle for multimodal imaging of cell death. Mol Imaging. 2013; 12: 182-90.
33. Lee S, Choi KY, Chung H, Ryu JH, Lee A, Koo H, et al. Real time, high resolution video imaging of apoptosis in single cells with a polymeric nanoprobe. Bioconjug Chem. 2011; 22: 125-31.
34. Choi KY, Jeon EJ, Yoon HY, Lee BS, Na JH, Min KH, et al. Theranostic nanoparticles based on PEGylated hyaluronic acid for the diagnosis, therapy and monitoring of colon cancer. Biomaterials. 2012; 33: 6186-93.
35. Dolmans DE, Fukumura D, Jain RK. Photodynamic therapy for cancer. Nat Rev Cancer. 2003; 3: 380-7.
36. Lee SJ, Koo H, Jeong H, Huh MS, Choi Y, Jeong SY, et al. Comparative study of photosensitizer loaded and conjugated glycol chitosan nanoparticles for cancer therapy. J Control Release. 2011; 152: 21-9.
37. Yoon HY, Koo H, Choi KY, Lee SJ, Kim K, Kwon IC, et al. Tumor-targeting hyaluronic acid nanoparticles for photodynamic imaging and therapy. Biomaterials. 2012; 33: 3980-9.
38. Shen J, Zhao L, Han G. Lanthanide-doped upconverting luminescent nanoparticle platforms for optical imaging-guided drug delivery and therapy. Adv Drug Deliv Rev. 2013; 65: 744-55.

39. Yang D, Ma P, Hou Z, Cheng Z, Li C, Lin J. Current advances in lanthanide ion (Ln(3+))-based upconversion nanomaterials for drug delivery. Chem Soc Rev. 2015; 44: 1416-48.

40. Park YI, Lee KT, Suh YD, Hyeon T. Upconverting nanoparticles: a versatile platform for wide-field two-photon microscopy and multi-modal in vivo imaging. Chem Soc Rev. 2015; 44: 1302-17.

41. Ma P, Xiao H, Li X, Li C, Dai Y, Cheng Z, et al. Rational design of multifunctional upconversion nanocrystals/polymer nanocomposites for cisplatin (IV) delivery and biomedical imaging. Adv Mater. 2013; 25: 4898-905.

42. Tian G, Zheng X, Zhang X, Yin W, Yu J, Wang D, et al. TPGS-stabilized NaYbF4:Er upconversion nanoparticles for dual-modal fluorescent/CT imaging and anticancer drug delivery to overcome multi-drug resistance. Biomaterials. 2015; 40: 107-16.

43. Wang C, Tao H, Cheng L, Liu Z. Near-infrared light induced in vivo photodynamic therapy of cancer based on upconversion nanoparticles. Biomaterials. 2011; 32: 6145-54.

44. Tian G, Ren W, Yan L, Jian S, Gu Z, Zhou L, et al. Red-emitting upconverting nanoparticles for photodynamic therapy in cancer cells under near-infrared excitation. Small. 2013; 9: 1929-38, 8.

45. Park YI, Kim JH, Lee KT, Jeon KS, Bin Na H, Yu JH, et al. Nonblinking and Nonbleaching Upconverting Nanoparticles as an Optical Imaging Nanoprobe and T1 Magnetic Resonance Imaging Contrast Agent. Adv Mater. 2009; 21: 4467-+.

46. Yang Y, Sun Y, Cao T, Peng J, Liu Y, Wu Y, et al. Hydrothermal synthesis of NaLuF4:153Sm,Yb,Tm nanoparticles and their application in dual-modality upconversion luminescence and SPECT bioimaging. Biomaterials. 2013; 34: 774-83.

47. Willmann JK, van Bruggen N, Dinkelborg LM, Gambhir SS. Molecular imaging in drug development. Nat Rev Drug Discov. 2008; 7: 591-607.

48. Yigit MV, Moore A, Medarova Z. Magnetic nanoparticles for cancer diagnosis and therapy. Pharm Res. 2012; 29: 1180-8.

49. Raymond KN, Pierre VC. Next generation, high relaxivity gadolinium MR1 agents. Bioconjug Chem. 2005; 16: 3-8.

50. Grange C, Geninatti-Crich S, Esposito G, Alberti D, Tei L, Bussolati B, et al. Combined delivery and magnetic resonance imaging of neural cell adhesion molecule-targeted doxorubicin-containing liposomes in experimentally induced Kaposi's sarcoma. Cancer Res. 2010; 70: 2180-90.

51. Shukla S, Steinmetz NF. Virus-based nanomaterials as positron emission tomography and magnetic resonance contrast agents: from technology development to translational medicine. Wiley Interdiscip Rev Nanomed Nanobiotechnol. 2015; 7: 708-21.

52. Bruckman MA, Hern S, Jiang K, Flask CA, Yu X, Steinmetz NF. Tobacco mosaic virus rods and spheres as supramolecular high-relaxivity MRI contrast agents. J Mater Chem B Mater Biol Med. 2013; 1: 1482-90.

53. Kobayashi T. Cancer hyperthermia using magnetic nanoparticles. Biotechnol J. 2011; 6: 1342-7.

54. Hayashi K, Nakamura M, Sakamoto W, Yogo T, Miki H, Ozaki S, et al. Superparamagnetic nanoparticle clusters for cancer theranostics combining magnetic resonance imaging and hyperthermia treatment. Theranostics. 2013; 3: 366-76.

55. Yu MK, Jeong YY, Park J, Park S, Kim JW, Min JJ, et al. Drug-loaded superparamagnetic iron oxide nanoparticles for combined cancer imaging and therapy in vivo. Angew Chem Int Ed Engl. 2008; 47: 5362-5.

56. Pack DW, Hoffman AS, Pun S, Stayton PS. Design and development of polymers for gene delivery. Nat Rev Drug Discov. 2005; 4: 581-93.

57. Yang H, Li Y, Li TT, Xu M, Chen Y, Wu CH, et al. Multifunctional Core/Shell Nanoparticles Cross-linked Polyetherimide-folic Acid as Efficient Notch-1 siRNA Carrier for Targeted Killing of Breast Cancer. Sci Rep. 2014; 4.

58. Carlsson CA. Imaging modalities in x-ray computerized tomography and in selected volume tomography. Phys Med Biol. 1999; 44: R23-56.

59. Xi D, Dong S, Meng XX, Lu QH, Meng LJ, Ye J. Gold nanoparticles as computerized tomography (CT) contrast agents. Rsc Adv. 2012; 2: 12515-24.

60. Kim D, Jeong YY, Jon S. A drug-loaded aptamer-gold nanoparticle bioconjugate for combined CT imaging and therapy of prostate cancer. ACS nano. 2010; 4: 3689-96.

61. Sun H, Zhu X, Lu PY, Rosato RR, Tan W, Zu Y. Oligonucleotide aptamers: new tools for targeted cancer therapy. Mol Ther Nucleic Acids. 2014 Aug 5; 3: e182.

62. Jaque D, Martinez Maestro L, del Rosal B, Haro-Gonzalez P, Benayas A, Plaza JL, et al. Nanoparticles for photothermal therapies. Nanoscale. 2014; 6: 9494-530.

63. Zhang X, Xing JZ, Chen J, Ko L, Amanie J, Gulavita S, et al. Enhanced radiation sensitivity in prostate cancer by gold-nanoparticles. Clin Invest Med. 2008; 31: E160-7.

64. Hainfeld JF, Slatkin DN, Smilowitz HM. The use of gold nanoparticles to enhance radiotherapy in mice. Phys Med Biol. 2004; Sep; 49: N309-N15.

65. Huang P, Bao L, Zhang C, Lin J, Luo T, Yang D, et al. Folic acid-conjugated silica-modified gold nanorods for X-ray/CT imaging-guided dual-mode radiation and photo-thermal therapy. Biomaterials. 2011; 32: 9796-809.

66. Phelps ME. PET: The merging of biology and imaging into molecular imaging. J Nucl Med. 2000; 41: 661-81.

67. Xiao Y, Hong H, Javadi A, Engle JW, Xu W, Yang Y, et al. Multifunctional unimolecular micelles for cancer-targeted drug delivery and positron emission tomography imaging. Biomaterials. 2012; 33: 3071-82.

68. Bartlett DW, Su H, Hildebrandt IJ, Weber WA, Davis ME. Impact of tumor-specific targeting on the biodistribution and efficacy of siRNA nanoparticles measured by multimodality in vivo imaging. Proc Natl Acad Sci U S A. 2007; 104: 15549-54.

69. Stride E, Saffari N. Microbubble ultrasound contrast agents: a review. Proc Inst Mech Eng H. 2003; 217: 429-47.

70. Qin S, Caskey CF, Ferrara KW. Ultrasound contrast microbubbles in imaging and therapy: physical principles and engineering. Phys Med Biol. 2009; 54: R27-57.

71. Bloch SH, Wan M, Dayton PA, Ferrara KW. Optical observation of lipid- and polymer-shelled ultrasound microbubble contrast agents. Appl Phys Lett. 2004; 84: 631-3.

72. Son S, Min HS, You DG, Kim BS, Kwon IC. Echogenic nanoparticles for ultrasound technologies: Evolution from diagnostic imaging modality to multimodal theranostic agent. Nano Today. 2014; 9: 525-40.

73. Min HS, You DG, Son S, Jeon S, Park JH, Lee S, et al. Echogenic Glycol Chitosan Nanoparticles for Ultrasound-Triggered Cancer Theranostics. Theranostics. 2015; 5: 1402-18.

74. Maeda H, Wu J, Sawa T, Matsumura Y, Hori K. Tumor vascular permeability and the EPR effect in macromolecular therapeutics: a review. J Control Release. 2000; 65: 271-84.

75. Min KH, Min HS, Lee HJ, Park DJ, Yhee JY, Kim K, et al. pH-controlled gas-generating mineralized nanoparticles: a theranostic agent for ultrasound imaging and therapy of cancers. ACS nano. 2015; 9: 134-45.

76. Choi BY, Park HJ, Hwang SJ, Park JB. Preparation of alginate beads for floating drug delivery system: effects of CO2 gas-forming agents. Int J Pharm. 2002; 239: 81-91.

77. Gerweck LE, Seetharaman K. Cellular pH gradient in tumor versus normal tissue: potential exploitation for the treatment of cancer. Cancer Res. 1996; 56: 1194-8.

78. Wikehooley JL, Haveman J, Reinhold HS. The Relevance of Tumor Ph to the Treatment of Malignant Disease. Radiother Oncol. 1984; 2: 343-66.

79. Goss SL, Lemons KA, Kerstetter JE, Bogner RH. Determination of calcium salt solubility with changes in pH and P-CO2, simulating varying gastrointestinal environments. J Pharm Pharmacol. 2007; 59: 1485-92.

80. Kennedy JE. High-intensity focused ultrasound in the treatment of solid tumours. Nat Rev Cancer. 2005; 5: 321-7.

81. Deckers R, Moonen CT. Ultrasound triggered, image guided, local drug delivery. J Control Release. 2010; 148: 25-33.

82. Ma M, Xu H, Chen H, Jia X, Zhang K, Wang Q, et al. A drug-perfluorocarbon nanoemulsion with an ultrathin silica coating for the synergistic effect of chemotherapy and ablation by high-intensity focused ultrasound. Adv Mater. 2014; 26: 7378-85.

83. Wang X, Chen HR, Zhang K, Ma M, Li FQ, Zeng DP, et al. An Intelligent Nanotheranostic Agent for Targeting, Redox-Responsive Ultrasound Imaging, and Imaging GuidedHigh- Intensity Focused Ultrasound Synergistic Therapy. Small. 2014; 10: 1403-11.